Parametric Rao Test for Multichannel Adaptive Signal Detection

KWANG JUNE SOHN

HONGBIN LI, Member, IEEE
Stevens Institute of Technology

BRAHAM HIMED, Fellow, IEEE
Air Force Research Laboratory

The parametric Rao test for a multichannel adaptive signal detection problem is derived by modeling the disturbance signal as a multichannel autoregressive (AR) process. Interestingly, the parametric Rao test takes a form identical to that of the recently introduced parametric adaptive matched filter (PAMF) detector for space-time adaptive processing (STAP) in airborne surveillance radar systems and other similar applications. The equivalence offers new insights into the performance and implementation of the PAMF detector. Specifically, the Rao/PAMF detector is asymptotically (for large samples) a parametric generalized likelihood ratio test (GLRT), due to an asymptotic equivalence between the Rao test and the GLRT. The asymptotic distribution of the Rao test statistic is obtained in closed form, which follows an exponential distribution under the null hypothesis H_0 and, respectively, a noncentral Chi-squared distribution with two degrees of freedom under the alternative hypothesis H_1. The noncentrality parameter of the noncentral Chi-squared distribution is determined by the output signal-to-interference-plus-noise ratio (SINR) of a temporal whitening filter. Since the asymptotic distribution under H_0 is independent of the unknown parameters, the Rao/PAMF asymptotically achieves constant false alarm rate (CFAR). Numerical results show that these results are accurate in predicting the performance of the parametric Rao/PAMF detector even with moderate data support.

Manuscript received August 25, 2005; revised May 6, 2006; released for publication August 26, 2006.

IEEE Log No. T-AES/43/3/908400.

Refereeing of this contribution was handled by M. Rangaswamy.

This work was supported by the Air Force Research Laboratory (AFRL) under Contract FA8750-05-2-0001.

Part of this work was presented at the 39th Asilomar Conference on Signals, Systems, and Computers, Pacific Grove, CA, Oct. 30–Nov. 2, 2005.

Authors' current addresses: K. J. Sohn and H. Li, Dept. of Electrical and Computer Engineering, Stevens Institute of Technology, Hoboken, NJ 07030, E-mail: (hli@stevens.edu); B. Himed, Signal Labs, Inc., 1950 Roland Clark Place, Suite 120, Reston, VA 20191.

I. INTRODUCTION

Multichannel signal detection is encountered in a wide variety of applications. In radar systems, sensor arrays are often used to facilitate the so-called space-time adaptive processing (STAP), which offers enhanced target discrimination capability compared with space- or time-only processing [1, 2]. In remote sensing systems, multispectral and hyperspectral sensors are used to collect spectral information across multiple spectral bands, which can be exploited for classification of different materials or detection of man-made objects on the ground [3, 4]. Other examples of applications include wireless communications, geolocation, sonars, audio and speech processing, and seismology [5–7].

STAP-based multichannel signal detectors have been successfully used to mitigate the effects of clutter and/or interference in radar, remote sensing, and communication systems [1–5]. However, traditional STAP detectors, including the well-known RMB detector by Reed, Mallett, and Brennan [8], Kelly's generalized likelihood ratio test (GLRT) [9], the adaptive matched filter (AMF) detector [10–12], and the adaptive coherence estimator (ACE) detector [13, 14], usually involve estimating and inverting a large-size space-time covariance matrix of the disturbance signal (viz., clutter, jamming, and noise) for each test cell using target-free training data. This entails high complexity and large training requirement. While the first difficulty may create real-time implementation burdens, the second implies that such covariance matrix based techniques may not be used in heterogeneous (due to varying terrain, high platform altitude, bistatic geometry, conformal array, among others) or dense-target environments, which offer limited training data.

Addressing the above issues has become an important topic in recent multichannel signal detection research. One effective way to reduce the computational and training requirement is to utilize a suitable parametric model for the disturbance signal and exploit the model for signal detection. For example, multichannel autoregressive (AR) models have been found to be very effective in representing the spatial and temporal correlation of the disturbance [15–18]. A parametric detector based on such a multichannel AR model is developed in [15], [16], which is referred to as the parametric adaptive matched filter (PAMF). The PAMF detector has been shown to significantly outperform the aforementioned covariance matrix based detectors for small training size at reduced complexity. Specifically, the PAMF detector models the disturbance as a multichannel AR process driven by a temporally white but spatially colored multichannel noise. While traditional STAP detectors perform joint space-time whitening (using an estimate of the space-time covariance matrix),

the PAMF detector adopts a two-step approach that involves temporal whitening via an inverse moving-average (MA) filter followed by spatial whitening. The parameters that need to be estimated are the AR coefficient matrices and the spatial covariance matrix of the driving multichannel noise, which are significantly fewer than what are involved in estimating the space-time covariance matrix. This is the essence behind the training and computational efficiency of the PAMF detector. The relationship and distinctions between the covariance matrix based detectors and the PAMF detector are further discussed in Section III.

Although intuitively sound, the PAMF detector was obtained in a heuristic approach by modifying the AMF test statistic. Specifically, it replaces the joint space-time whitening incurred by the AMF detector with two separate whitening procedures in time and space as discussed above. The test threshold and false alarm and detection probabilities were determined primarily by computer simulation, due to limited analysis available for the PAMF detector.

In the work presented here, we derive the parametric Rao test for multichannel signal detection. The generic Rao test is known to offer a standard solution to a class of parameter testing problems. It is easier to derive and implement than the GLRT, and is also asymptotically (large-sample in the number of temporal observations and/or training signals) equivalent to the latter. The Rao test was recently used to develop detectors for several other problems [19, 20]. A detailed discussion on the attributes of a generic Rao test can be found in [7].

Our parametric Rao test differs from the generic one for multichannel signal detection in that we make explicit use of a multichannel AR model for the disturbance signal. We show that, interestingly, the parametric Rao test takes a form identical to that of the PAMF detector. The only difference is that we use a maximum likelihood (ML) based estimator that involves using both test and training signals for parameter estimation, whereas the estimators in [16] use only training signals for parameter estimation. If the ML estimator is utilized, the parametric Rao/PAMF detector is asymptotically a parametric GLRT. Under the conditions stated in Section II, the asymptotic distribution of the test statistic under both hypotheses is obtained in closed form, which can be used to set the test threshold and compute the corresponding detection and false alarm probabilities. Since the asymptotic distribution under H_0 is independent of the unknown parameters, the parametric Rao/PAMF detector asymptotically achieves constant false alarm rate (CFAR). Numerical results are presented, which show that our asymptotic results are accurate in predicting the performance of the Rao/PAMF detector even when the data size is modest.

The remainder of the paper is organized as follows. Section II contains the data model and problem statement. The covariance-matrix based detectors and the PAMF detector are briefly reviewed in Section III. Our main results are summarized in Section IV. In particular, Section IVA contains a summary of the parametric test statistic, while Section IVB includes our asymptotic analysis. Details of the technical developments of the results reported in Section IV are found in Appendices A to C. Numerical results are presented in Section V. Finally, Section VI contains our concluding remarks.

Notation: Vectors (matrices) are denoted by boldface lower (upper) case letters, all vectors are column vectors, superscripts $(\cdot)^{\mathrm{T}}$, $(\cdot)^*$, and $(\cdot)^{\mathrm{H}}$ denote transpose, complex conjugate, and complex conjugate transpose, respectively, $\mathcal{CN}(\boldsymbol{\mu}, \mathbf{R})$ denotes the multivariate complex Gaussian distribution with mean vector $\boldsymbol{\mu}$ and covariance matrix $\mathbf{R}$, $\otimes$ denotes the Kronecker product, vec$(\cdot)$ denotes the operation of stacking the columns of a matrix on top of each other, $\mathbb{C}$ denotes the complex number field, $\Re\{\cdot\}$ takes the real part of the argument, and $\Im\{\cdot\}$ takes the imaginary part.

II. DATA MODEL AND PROBLEM STATEMENT

The problem under consideration involves detecting a known multichannel signal with unknown amplitude in the presence of spatially and temporally correlated disturbance (e.g., [1]):

$$\begin{aligned} H_0 &: \quad \mathbf{x}_0(n) = \mathbf{d}(n), \qquad n = 0, 1, \ldots, N-1 \\ H_1 &: \quad \mathbf{x}_0(n) = \alpha \mathbf{s}(n) + \mathbf{d}(n), \qquad n = 0, 1, \ldots, N-1 \end{aligned} \tag{1}$$

where all vectors are $J \times 1$ vectors, J denotes the number of spatial channels, and N is the number of temporal observations. Henceforth, $\mathbf{x}_0(n)$ is called the test signal, $\mathbf{s}(n)$ is the signal to be detected with amplitude α, and $\mathbf{d}(n)$ is the disturbance signal that may be correlated in space and time. In addition to the test signal, it is assumed that a set of target-free training or secondary data vectors $\mathbf{x}_k(n)$, $k = 1, 2, \ldots, K$ and $n = 0, 1, \ldots, N-1$, are available to assist signal detection.

Define the following $JN \times 1$ space-time vectors:

$$\begin{aligned} \mathbf{s} &= [\mathbf{s}^{\mathrm{T}}(0), \mathbf{s}^{\mathrm{T}}(1), \ldots, \mathbf{s}^{\mathrm{T}}(N-1)]^{\mathrm{T}} \\ \mathbf{d} &= [\mathbf{d}^{\mathrm{T}}(0), \mathbf{d}^{\mathrm{T}}(1), \ldots, \mathbf{d}^{\mathrm{T}}(N-1)]^{\mathrm{T}} \\ \mathbf{x}_k &= [\mathbf{x}_k^{\mathrm{T}}(0), \mathbf{x}_k^{\mathrm{T}}(1), \ldots, \mathbf{x}_k^{\mathrm{T}}(N-1)]^{\mathrm{T}} \\ k &= 0, 1, \ldots, K. \end{aligned} \tag{2}$$

Equation (1) can be more compactly written as

$$\begin{aligned} H_0 &: \quad \mathbf{x}_0 = \mathbf{d} \\ H_1 &: \quad \mathbf{x}_0 = \alpha \mathbf{s} + \mathbf{d}. \end{aligned} \tag{3}$$

Clearly, the composite hypothesis testing problem (1) or (3) is also a two-sided parameter testing problem that tests $\alpha = 0$ against $\alpha \neq 0$. The general assumptions in the literature are ([1–4, 8–16]) the following.

AS1: The signal vector $\mathbf{s}$ is deterministic and known to the detector.

AS2: The signal amplitude α is complex valued, deterministic, and unknown.

AS3: The secondary data $\{\mathbf{x}_k\}_{k=1}^K$ and the disturbance signal $\mathbf{d}$ (equivalently, $\mathbf{x}_0$ under H_0) are independent and identically distributed (IID) with distribution $\mathcal{CN}(\mathbf{0},\mathbf{R})$, where $\mathbf{R}$ is the unknown space-time covariance matrix.

In particular, the above signal detection problem occurs in an airborne STAP radar system with J array channels and a coherent processing interval (CPI) of N pulse repetition intervals (PRIs). The disturbance $\mathbf{d}(n)$ consists of ground clutter, jamming, and thermal noise, while $\mathbf{s}(n)$ is called the target space-time steering vector. For a uniform equi-spaced linear array,[1] the steering vector is given by [16]:

$$\mathbf{s}(\omega_s,\omega_d) = \mathbf{s}_t(\omega_d) \otimes \mathbf{s}_s(\omega_s) \tag{4}$$

where $\mathbf{s}_s(\omega_s)$ denotes the $J \times 1$ spatial steering vector:

$$\mathbf{s}_s(\omega_s) = \frac{1}{\sqrt{J}}[1, e^{j\omega_s}, \ldots, e^{j\omega_s(J-1)}]^{\mathrm{T}} \tag{5}$$

and $\mathbf{s}_t(\omega_d)$ denotes the $N \times 1$ temporal steering vector:

$$\mathbf{s}_t(\omega_d) = \frac{1}{\sqrt{N}}[1, e^{j\omega_d}, \ldots, e^{j\omega_d(N-1)}]^{\mathrm{T}} \tag{6}$$

where ω_s and ω_d denote the normalized target spatial and Doppler frequencies, respectively.

While Assumptions AS1 to AS3 are standard (e.g., [1–4, 8–14]), we further assume the following:

AS4: The disturbance signal $\mathbf{d}(n)$ can be modeled as a multichannel AR(P) process with known model order P but unknown AR coefficient matrices and spatial covariance (see Remark 1 below for additional comments on this assumption).

Based on Assumption AS4, the secondary data $\{\mathbf{x}_k\}_{k=1}^K$ are represented as

$$\mathbf{x}_k(n) = -\sum_{p=1}^{P} \mathbf{A}^{\mathrm{H}}(p)\mathbf{x}_k(n-p) + \boldsymbol{\varepsilon}_k(n), \qquad k = 1,2,\ldots,K \tag{7}$$

where $\{\mathbf{A}^{\mathrm{H}}(p)\}_{p=1}^P$ denote the $J \times J$ AR coefficient matrices, and $\boldsymbol{\varepsilon}_k(n)$ denote the driving multichannel spatial noise vectors that are temporally white but spatially colored Gaussian noise: $\boldsymbol{\varepsilon}_k(n) \sim \mathcal{CN}(\mathbf{0},\mathbf{Q})$, where $\mathbf{Q}$ denotes the $J \times J$ spatial covariance matrix. Meanwhile, the test signal $\mathbf{x}_0$ is given by

$$\begin{aligned}\mathbf{x}_0(n) - \alpha\mathbf{s}(n) &= -\sum_{p=1}^{P} \mathbf{A}^{\mathrm{H}}(p)\{\mathbf{x}_0(n-p) - \alpha\mathbf{s}(n-p)\} + \boldsymbol{\varepsilon}_0(n)\end{aligned} \tag{8}$$

where $\alpha = 0$ under H_0, $\alpha \neq 0$ under H_1, and $\boldsymbol{\varepsilon}_0(n) \sim \mathcal{CN}(\mathbf{0},\mathbf{Q})$. Let $\tilde{\mathbf{s}}(n)$ denote a regression on $\mathbf{s}(n)$ and $\tilde{\mathbf{x}}_0(n)$ a regression on $\mathbf{x}_0(n)$ under H_1:

$$\tilde{\mathbf{s}}(n) = \mathbf{s}(n) + \sum_{p=1}^{P} \mathbf{A}^{\mathrm{H}}(p)\mathbf{s}(n-p) \tag{9}$$

$$\tilde{\mathbf{x}}_0(n) = \mathbf{x}_0(n) + \sum_{p=1}^{P} \mathbf{A}^{\mathrm{H}}(p)\mathbf{x}_0(n-p). \tag{10}$$

Then, the driving noise in (8) can be alternatively expressed as

$$\boldsymbol{\varepsilon}_0(n) = \tilde{\mathbf{x}}_0(n) - \alpha\tilde{\mathbf{s}}(n). \tag{11}$$

The problem of interest is to develop a decision rule for the above composite hypothesis testing problem using the test and training signals as well as exploiting the multichannel parametric AR model.

REMARK 1 We clarify that our goal here is not to justify whether AR models are appropriate or not for STAP applications. An answer to the question can be found in [16], where it is shown that low-order multichannel AR models are very powerful and efficient in capturing the temporal and spatial correlation of the disturbance and, hence, can greatly help signal detection in airborne STAP systems. As stated above, our problem is how to exploit such a parametric model to solve the composite testing problem. The assumption that the model order P is known is only used to simplify our presentation. In practice, the model order has to be estimated, and a variety of model order selection techniques, such as the Akaike information criterion (AIC) and the minimum description length (MDL) based techniques (e.g., [21] and references therein), are available for this task. Since such techniques may overestimate or underestimate the true model order, a relevant problem is how the proposed detector performs when overestimation or underestimation occurs (also see [22]). This is investigated in Section V. Finally, it is also possible to formulate the problem to include P as another parameter to be estimated. We do not follow such an approach in order to focus on the relations between the parametric Rao test and the PAMF detector, which also assumes that a prior estimate of P is available.

[1]Note that the results presented in this paper apply to any array configurations, as long as the steering vector is known (cf. Assumption AS1).

III. PRIOR SOLUTIONS

A number of solutions to the above problem have been developed. If the space-time covariance matrix $\mathbf{R}$ is known exactly, the optimum detector that maximizes the output SINR is the matched filter (MF) [12]:

$$T_{\mathrm{MF}} = \frac{|\mathbf{s}^{\mathrm{H}}\mathbf{R}^{-1}\mathbf{x}_0|^2}{\mathbf{s}^{\mathrm{H}}\mathbf{R}^{-1}\mathbf{s}} \underset{H_0}{\overset{H_1}{\gtrless}} \gamma_{\mathrm{MF}} \tag{12}$$

where γ_{MF} denotes the MF threshold. The MF detector is obtained by a GLRT approach (e.g., [7]), by which the ML estimate of the unknown amplitude α is first estimated and then substituted back into the likelihood ratio to form a test statistic. It should be noted that the MF detector cannot be implemented in real applications since $\mathbf{R}$ is unknown. However, it provides a baseline for performance comparison when considering any realizable detection scheme.

In practice, the unknown $\mathbf{R}$ can be replaced by some estimate, such as the sample covariance matrix obtained from the secondary data:

$$\hat{\mathbf{R}} = \frac{1}{K}\sum_{k=1}^{K}\mathbf{x}_k\mathbf{x}_k^{\mathrm{H}}. \tag{13}$$

Using $\hat{\mathbf{R}}$ in (12) leads to the so-called AMF detector [10–12]:

$$T_{\mathrm{AMF}} = \frac{|\mathbf{s}^{\mathrm{H}}\hat{\mathbf{R}}^{-1}\mathbf{x}_0|^2}{\mathbf{s}^{\mathrm{H}}\hat{\mathbf{R}}^{-1}\mathbf{s}} \underset{H_0}{\overset{H_1}{\gtrless}} \gamma_{\mathrm{AMF}} \tag{14}$$

where γ_{AMF} denotes the AMF threshold.

Alternatively, one can treat both α and $\mathbf{R}$ as unknowns and estimate them successively by ML. Such a GLRT approach was pursued by Kelly [9], which gives the following Kelly test:

$$T_{\mathrm{Kelly}} = \frac{|\mathbf{s}^{\mathrm{H}}\hat{\mathbf{R}}^{-1}\mathbf{x}_0|^2}{(\mathbf{s}^{\mathrm{H}}\hat{\mathbf{R}}^{-1}\mathbf{s})(K + \mathbf{x}_0^{\mathrm{H}}\hat{\mathbf{R}}^{-1}\mathbf{x}_0)} \underset{H_0}{\overset{H_1}{\gtrless}} \gamma_{\mathrm{Kelly}} \tag{15}$$

where γ_{Kelly} denotes the corresponding threshold.

The AMF and Kelly tests are both CFAR detectors, which is a desirable property in radar systems. However, they also entail a large training requirement. In particular, the sample covariance matrix $\hat{\mathbf{R}}$ has to be inverted, which imposes a constraint on the training size

$$K \geq JN \tag{16}$$

to ensure a full-rank $\hat{\mathbf{R}}$. The Reed-Brennan rule [8] suggests that at least $K \geq (2JN - 3)$ target-free secondary data vectors are needed to obtain expected performance within 3 dB from the optimum MF detector. Such a training requirement may be difficult to meet, especially in nonhomogeneous or dense-target environments. Besides excessive training, the computational complexity of these detectors is also high, since $\hat{\mathbf{R}}$ has to be computed and inverted for each CPI.

While the AMF and Kelly tests may be called covariance matrix based techniques as they both involve computing and inverting $\hat{\mathbf{R}}$, the recently introduced PAMF detector [16] utilizes a multichannel AR(P) model that allows spatial/temporal whitening to be implemented in a multichannel time-series fashion (see [16] for details):

$$T_{\mathrm{PAMF}} = \frac{\left|\sum_{n=P}^{N-1}\hat{\tilde{\mathbf{s}}}_{\mathrm{P}}^{\mathrm{H}}(n)\hat{\mathbf{Q}}_{\mathrm{P}}^{-1}\hat{\tilde{\mathbf{x}}}_{0,\mathrm{P}}(n)\right|^2}{\sum_{n=P}^{N-1}\hat{\tilde{\mathbf{s}}}_{\mathrm{P}}^{\mathrm{H}}(n)\hat{\mathbf{Q}}_{\mathrm{P}}^{-1}\hat{\tilde{\mathbf{s}}}_{\mathrm{P}}(n)} \underset{H_0}{\overset{H_1}{\gtrless}} \gamma_{\mathrm{PAMF}} \tag{17}$$

where $\hat{\mathbf{Q}}_{\mathrm{P}}$ denotes an estimate of the spatial covariance matrix $\mathbf{Q}$, $\hat{\tilde{\mathbf{x}}}_{0,\mathrm{P}}(n)$ and $\hat{\tilde{\mathbf{s}}}_{\mathrm{P}}(n)$ are the temporally whitened test signal and steering vector, respectively; these are whitened using an inverse AR(P) filter (i.e., a multichannel MA filter) whose parameters, along with $\hat{\mathbf{Q}}_{\mathrm{P}}$, are estimated from the secondary data. In contrast to simultaneous spatio-temporal whitening used in the AMF and Kelly tests, the PAMF detector performs whitening in two distinct steps: temporal whitening followed by spatial whitening. The parametric approach offers savings in both training and computation, since the parameters to be estimated are significantly fewer, compared with covariance matrix based approaches.

IV. PARAMETRIC RAO TEST

A. Test Statistic

The derivation of the parametric Rao test that takes into account Assumptions AS1 to AS4 in Section II is presented in Appendix B, which in turns relies on the ML estimates of the nuisance parameters (i.e., parameters associated with the disturbance signal) that are obtained in Appendix A. The test is given by[2]

$$T_{\mathrm{Rao}} = \frac{2\left|\sum_{n=P}^{N-1}\hat{\tilde{\mathbf{s}}}^{\mathrm{H}}(n)\hat{\mathbf{Q}}^{-1}\hat{\tilde{\mathbf{x}}}_0(n)\right|^2}{\sum_{n=P}^{N-1}\hat{\tilde{\mathbf{s}}}^{\mathrm{H}}(n)\hat{\mathbf{Q}}^{-1}\hat{\tilde{\mathbf{s}}}(n)} \underset{H_0}{\overset{H_1}{\gtrless}} \gamma_{\mathrm{Rao}} \tag{18}$$

where γ_{Rao} denotes the test threshold, which can be set by using the results in Section IVB, $\hat{\tilde{\mathbf{s}}}(n)$ and $\hat{\tilde{\mathbf{x}}}_0(n)$ denote, respectively, the steering vector and test signal that have been whitened temporally, and additional spatial whitening is provided by $\hat{\mathbf{Q}}^{-1}$, which is the inverse of the ML estimate of the spatial covariance matrix to be specified next.

Specifically, the temporally whitened steering vector and test signal in (18) are obtained as follows:

$$\hat{\tilde{\mathbf{s}}}(n) = \mathbf{s}(n) + \sum_{p=1}^{P}\hat{\mathbf{A}}^{\mathrm{H}}(p)\mathbf{s}(n-p) \tag{19}$$

[2]Although the factor of 2 on the test statistic can be absorbed by the test threshold, it is retained to keep the asymptotic distribution of the test statistic more compact. See Section IVB.

$$\hat{\tilde{\mathbf{x}}}_0(n) = \mathbf{x}_0(n) + \sum_{p=1}^{P} \hat{\mathbf{A}}^{\mathrm{H}}(p)\mathbf{x}_0(n-p) \tag{20}$$

where $\hat{\mathbf{A}}^{\mathrm{H}}(p)$ denotes the ML estimate of the AR coefficient matrix $\mathbf{A}^{\mathrm{H}}(p)$.

To present the ML estimates more compactly, let

$$\mathbf{A}^{\mathrm{H}} = [\mathbf{A}^{\mathrm{H}}(1), \mathbf{A}^{\mathrm{H}}(2), \ldots, \mathbf{A}^{\mathrm{H}}(P)] \in \mathbb{C}^{J \times JP} \tag{21}$$

which contains all the coefficient matrices involved in the Pth order AR model, and

$$\mathbf{y}_k(n) = [\mathbf{x}_k^{\mathrm{T}}(n-1), \mathbf{x}_k^{\mathrm{T}}(n-2), \ldots, \mathbf{x}_k^{\mathrm{T}}(n-P)]^{\mathrm{T}} \qquad k = 0, 1, \ldots, K \tag{22}$$

which contains the regression subvectors formed from the test signal $\mathbf{x}_0$ or the kth training signal $\mathbf{x}_k$. We first compute the following correlation matrices:

$$\hat{\mathbf{R}}_{xx} = \sum_{n=P}^{N-1} \sum_{k=0}^{K} \mathbf{x}_k(n)\mathbf{x}_k^{\mathrm{H}}(n) \tag{23}$$

$$\hat{\mathbf{R}}_{yy} = \sum_{n=P}^{N-1} \sum_{k=0}^{K} \mathbf{y}_k(n)\mathbf{y}_k^{\mathrm{H}}(n) \tag{24}$$

$$\hat{\mathbf{R}}_{yx} = \sum_{n=P}^{N-1} \sum_{k=0}^{K} \mathbf{y}_k(n)\mathbf{x}_k^{\mathrm{H}}(n). \tag{25}$$

Then, the ML estimates of the AR coefficients $\mathbf{A}^{\mathrm{H}}$ and the spatial covariance matrix $\mathbf{Q}$ are given by (see Appendix A)

$$\hat{\mathbf{A}}^{\mathrm{H}} = -\hat{\mathbf{R}}_{yx}^{\mathrm{H}}\hat{\mathbf{R}}_{yy}^{-1} \tag{26}$$

$$\hat{\mathbf{Q}} = \frac{1}{(K+1)(N-P)}(\hat{\mathbf{R}}_{xx} - \hat{\mathbf{R}}_{yx}^{\mathrm{H}}\hat{\mathbf{R}}_{yy}^{-1}\hat{\mathbf{R}}_{yx}). \tag{27}$$

REMARK 2 The PAMF detector also involves estimating the AR coefficients $\mathbf{A}^{\mathrm{H}}$ and the spatial covariance matrix $\mathbf{Q}$ [16]. Several estimators were suggested, including the Strand-Nuttall algorithm and the least-squares (LS) estimators. The LS estimator was observed to yield better performance. Our ML estimator is similar to the LS estimator except that we use both the test and training signals to obtain parameter estimates, whereas the latter utilizes only the training signals for parameter estimation. A subscript "P" is therefore used for the parameter estimates in (17) to indicate the difference. Note that with the ML estimator, it is possible to derive parameter estimates exclusively from the test signal, thus obviating the need for training. This could be advantageous especially in highly heterogeneous environments where it is difficult to obtain training signals that are IID with respect to the disturbance in the test signal. The detection performance of the parametric Rao detector in the absence of training will be explored elsewhere. We would like to point out that our approach is similar to Kelly's GLRT [9], which also employs both the test and training signals for parameter estimation. However, we stress that Kelly's GLRT does not exploit the multichannel parametric model as shown in (7) and (8).

REMARK 3 By comparing the parametric Rao test statistic (18) and the PAMF test statistic (17), we can quickly see that if both detectors use the ML estimator for parameter estimation, they are identical except for a scaling factor of 2. Hence, under the conditions stated in Section II, the PAMF detector is a parametric Rao detector. Since the parametric Rao test is asymptotically equivalent to the parametric GLRT,[3] the PAMF detector, with the ML parameter estimates, is also an asymptotic parametric GLRT. As we see in Section IVB, the equivalence offers additional insights into the performance and implementation of the PAMF detector.

REMARK 4 It should be noted that similar to other STAP detectors, the parametric Rao test is adaptive in that the detector is data dependent, as evident in (18)–(27), which is in contrast to data independent detector (e.g., a correlator). This shall not be confused with recursive adaptive implementation. Although recursive adaptive implementation of the parametric Rao test would be of interest in a real-time system, it is beyond the scope of the current paper.

B. Asymptotic Analysis

As shown in Appendix C, the asymptotic distribution of the Rao/PAMF test statistic is given by

$$T_{\mathrm{Rao}} \overset{a}{\sim} \begin{cases} \chi_2^2, & \text{under } H_0 \\ \chi_2'^2(\lambda), & \text{under } H_1 \end{cases} \tag{28}$$

where χ_2^2 denotes the central Chi-squared distribution with 2 degrees of freedom and $\chi_2'^2(\lambda)$ the noncentral Chi-squared distribution with 2 degrees of freedom and noncentrality parameter λ:

$$\lambda = 2|\alpha|^2 \sum_{n=P}^{N-1} \tilde{\mathbf{s}}^{\mathrm{H}}(n)\mathbf{Q}^{-1}\tilde{\mathbf{s}}(n) \tag{29}$$

where $\tilde{\mathbf{s}}(n)$ is the temporally whitened steering vector given by (9). Note that λ is related to the SINR at the output of the temporal whitening filter. Recall that a χ_2^2 random variable is equivalent to an exponential random variable with probability density function (pdf) given by

$$f_{\chi_2^2}(x) = \tfrac{1}{2}\exp(-\tfrac{1}{2}x), \qquad x \geq 0. \tag{30}$$

[3]The parametric GLRT is different from Kelly's GLRT in that the former takes into account the parametric model in Section II, while the latter does not.

The pdf of $\chi_2'^2(\lambda)$ is given by [7]

$$f_{\chi_2'^2(\lambda)}(x) = \tfrac{1}{2}\exp[-\tfrac{1}{2}(x+\lambda)]I_0\left(\sqrt{\lambda x}\right), \qquad x \geq 0 \tag{31}$$

where $I_0(u)$ is the modified Bessel function of the first kind and zeroth order defined by

$$I_0(u) = \frac{1}{\pi}\int_0^{\pi} \exp(u\cos\theta)d\theta = \sum_{k=0}^{\infty} \frac{(\frac{1}{4}u^2)^k}{(k!)^2}. \tag{32}$$

The above distributions can be employed to set the Rao test threshold for a given probability of false alarm, as well as to compute the detection and false alarm probabilities, etc. For a given threshold, the probability of false alarm is given by

$$P_{\mathrm{f}} = \int_{\gamma_{\mathrm{Rao}}}^{\infty} f_{\chi_2^2}(x)dx = \exp(-\tfrac{1}{2}\gamma_{\mathrm{Rao}}) \tag{33}$$

which can easily be inverted to find the test threshold γ_{Rao} for a given P_{f}. In addition, the probability of detection is given by

$$P_{\mathrm{d}} = \int_{\gamma_{\mathrm{Rao}}}^{\infty} \tfrac{1}{2}\exp[-\tfrac{1}{2}(x+\lambda)]I_0\left(\sqrt{\lambda x}\right)dx \tag{34}$$

for a given test threshold γ_{Rao}.

REMARK 5 The asymptotic distribution under H_0 is independent of the unknown parameters. The probability of false alarm in (33) depends only on the test threshold, which is a design parameter. It is evident that the Rao/PAMF test asymptotically achieves CFAR.

REMARK 6 The above analysis holds under Assumptions AS1 to AS4 of Section II with one exception. In particular, since the ML parameter estimates are asymptotically Gaussian irrespective of the distribution of the observed data, the above analysis still holds if the Gaussian assumption in AS3 is dropped. This also explains why it has been observed in several studies that the PAMF detector obtains good performance even with non-Gaussian observations (see, e.g., [15]).

V. NUMERICAL RESULTS

In the following, we present our numerical results of the parametric Rao/PAMF detector obtained by computer simulation and by the above asymptotic analysis. In addition, the performance of the MF (12) and AMF (14) detectors, which can be computed analytically, is included for comparison. For easy reference, Appendix D contains a brief summary of relevant results that are used to compute the performance of the two detectors. We reiterate that the MF detector serves as a baseline only. We do not consider Kelly's GLRT since a detailed comparison between the GLRT and AMF detectors can be found in [12]. In the following, the disturbance signal is generated as a multichannel AR(2) process with randomly generated AR coefficients $\mathbf{A}$ and a spatial covariance matrix $\mathbf{Q}$. In particular, $\mathbf{A}$ and $\mathbf{Q}$ are selected to ensure that $\mathbf{Q}$ is a valid covariance matrix and, furthermore, $\mathbf{A}$ is chosen to ensure that the resulting AR process is stable. Once $\mathbf{A}$ and $\mathbf{Q}$ are selected, they are fixed in all trials. The signal vector $\mathbf{s}$ is generated as in (4) with randomly chosen normalized spatial and Doppler frequencies. The SINR is defined as

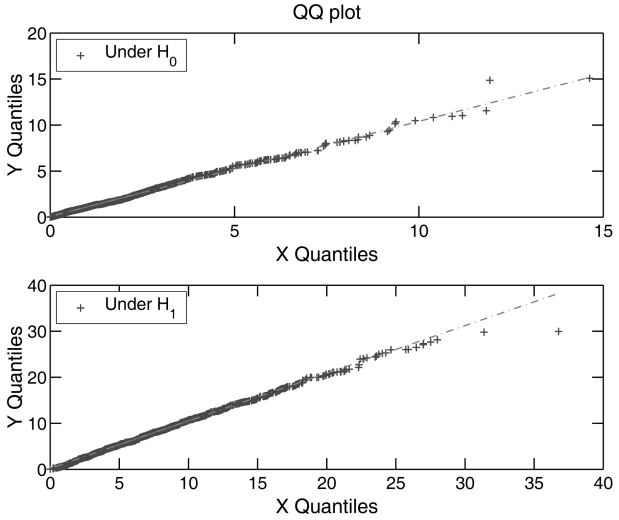

Fig. 1. Quantile-quantile plot of parametric Rao/PAMF test statistic and its asymptotic distribution under H_0 (upper plot) and H_1 (lower plot), respectively, with $J = 4$, $N = 32$, $K = 8$. Specifically, x-axis shows ordered samples of parametric Rao/PAMF test statistic, while y-axis shows ordered samples of asymptotic distribution.

$$\mathrm{SINR} = |\alpha|^2\mathbf{s}^{\mathrm{H}}\mathbf{R}^{-1}\mathbf{s} \tag{35}$$

where $\mathbf{R}$ is the $JN \times JN$ joint space-time covariance matrix of the disturbance $\mathbf{d}$, which can be determined once $\mathbf{A}$ and $\mathbf{Q}$ are selected (the details are not shown for simplicity). To numerically set the threshold for the parametric Rao/PAMF detector, a total of 5×10^4 trials are run. Meanwhile, to determine P_{d} for a given threshold, a total of 10^4 trials are run for each SINR.

First, we consider the asymptotic distribution of the parametric Rao/PAMF test statistic obtained in Section IVB. Fig. 1 depicts the quantile-quantile plot of the Rao/PAMF test statistic under both hypotheses against the corresponding asymptotic distribution when $J = 4$, $N = 32$, and $K = 8$, a case with limited training. It is seen that even with a relatively small data size, the asymptotic distribution matches well the sample test statistics, with only some minor deviation at the tail portion.

Next, we examine the receiver operating characteristic (ROC) [7] of the parametric Rao/PAMF detector. The parameters used in the simulation are $J = 4$, $N = 32$, and $K = 256$. Fig. 2 depicts the ROC curves for the parametric Rao/PAMF test obtained by

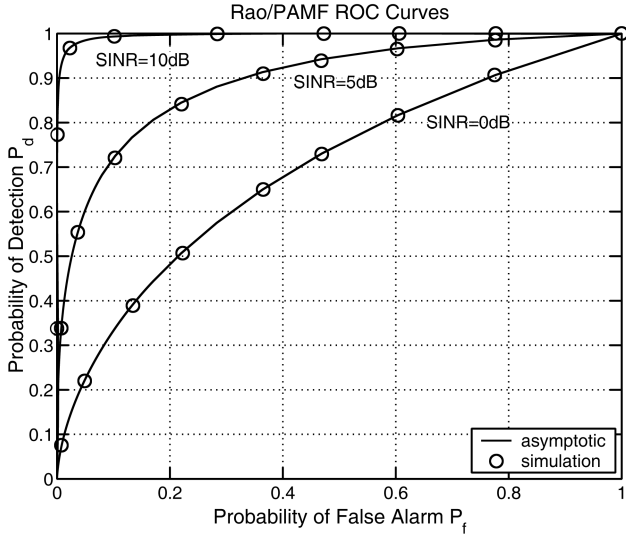

Fig. 2. ROC curves of parametric Rao/PAMF detector at various input SINR when $J = 4$, $N = 32$, $K = 256$.

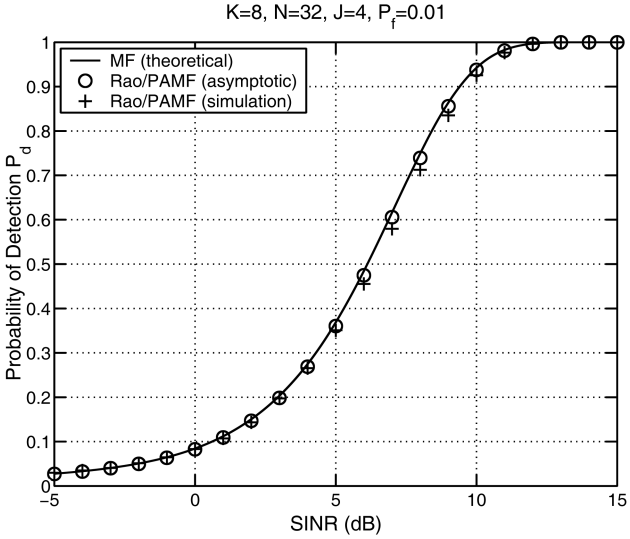

Fig. 4. Probability of detection P_{d} versus input SINR when $P_{\mathrm{f}} = 0.01$, $J = 4$, $N = 32$, $K = 8$. Note that AMF detector is not included since it cannot be implemented for such a small K.

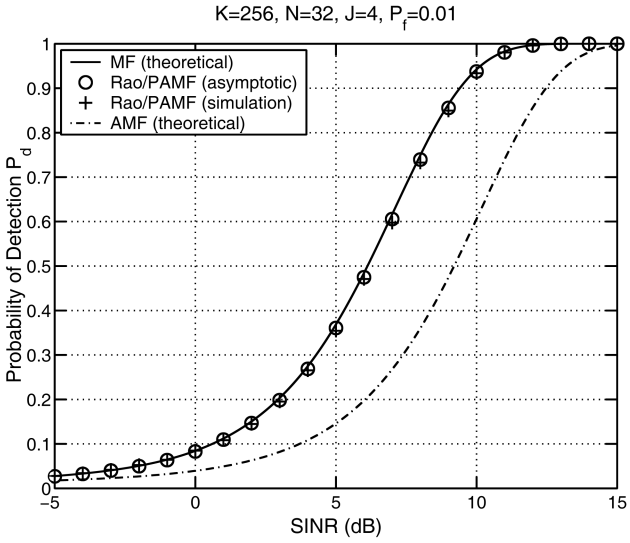

Fig. 3. Probability of detection P_{d} versus input SINR when $P_{\mathrm{f}} = 0.01$, $J = 4$, $N = 32$, $K = 256$.

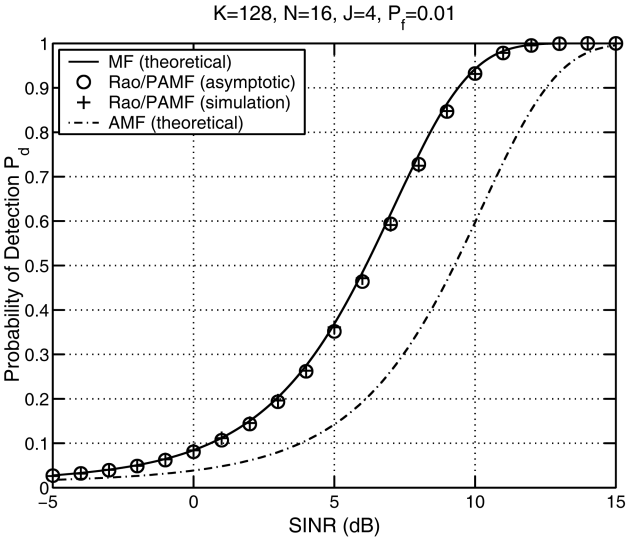

Fig. 5. Probability of detection P_{d} versus input SINR when $P_{\mathrm{f}} = 0.01$, $J = 4$, $N = 16$, $K = 128$.

simulation and asymptotic analysis for SINR values of 0, 5, and 10 dB. It is seen that the simulation results match those obtained by asymptotic analysis.

Figs. 3–6 depict the probability of detection P_{d} versus SINR for the MF, AMF, and the parametric Rao/PAMF detectors under various conditions that are specified below the figures. In particular, Figs. 3 and 5 correspond to the case with adequate training, for which the Reed-Brennan rule is satisfied (see discussions in Section III), whereas Figs. 4 and 6 correspond to the case with limited training, for which the AMF detector does not even exist, since the training size $K = 8$ is too small to meet the minimum training condition (16). An examination of these figures reveals the following.

1) When the assumptions of Section II are met, the asymptotic analysis provides a quite accurate prediction of the performance of the parametric Rao/PAMF detectors. The gap between the asymptotic and simulated results is seen to widen as K and/or N decreases. But even for the most challenging case with $K = 8$ and $N = 16$, the gap is about 0.5 dB, as shown in Fig. 6.

2) The parametric Rao/PAMF detector is very close to the optimum MF detector. The gap between the two detectors closes with increasing K and/or N.

3) The parametric Rao/PAMF detector outperforms the AMF detector by 2 to 3 dB when the Reed-Brennan rule is marginally satisfied. This agrees with earlier observations made in [16].

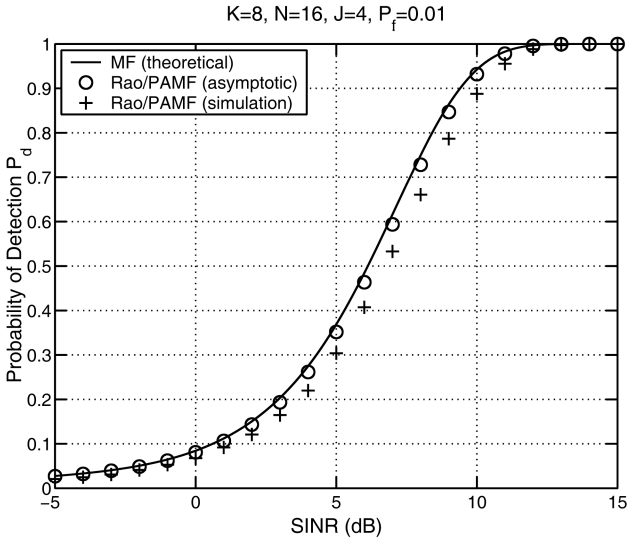

Fig. 6. Probability of detection P_d versus input SINR when $P_f = 0.01$, $J = 4$, $N = 16$, $K = 8$. Note that AMF detector is not included since it cannot be implemented for such a small K.

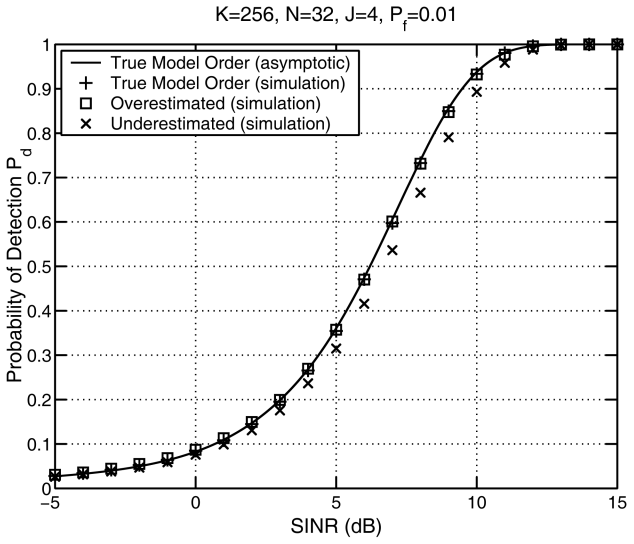

Fig. 7. Probability of detection P_d versus input SINR of parametric Rao/PAMF detector when model order of multichannel AR process used for computing test statistic is true ($P = 2$), underestimated (assuming $P = 1$), and overestimated (assuming $P = 3$), along with $P_f = 0.01$, $J = 4$, $N = 32$, $K = 256$.

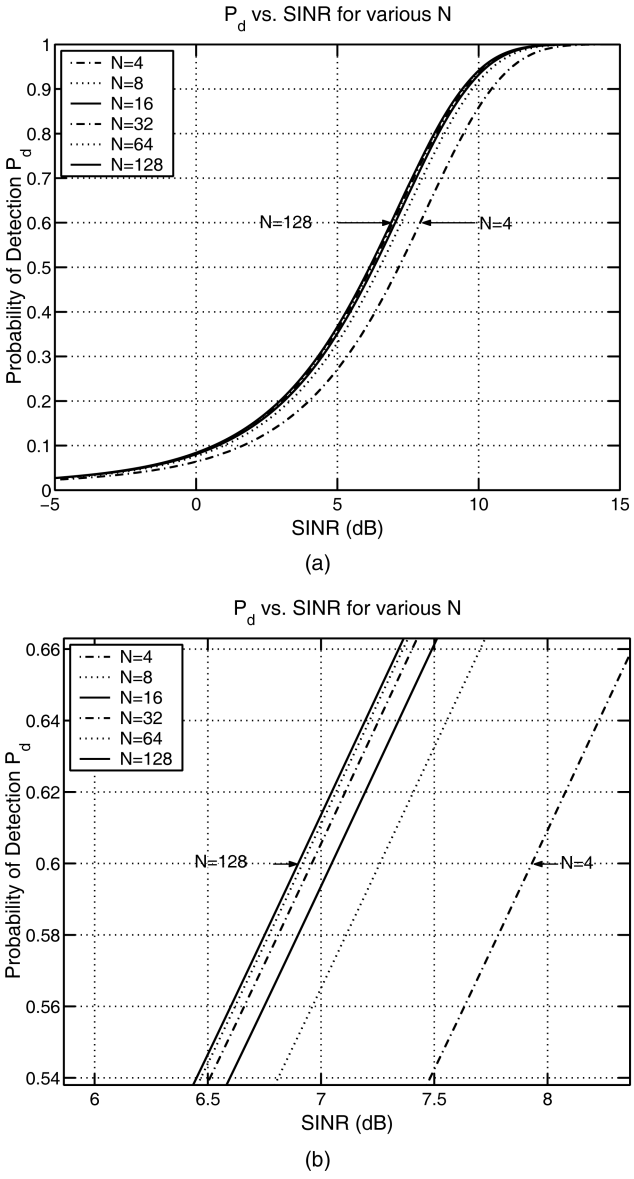

Fig. 8. (a) Impact of pulse number N on parametric Rao/PAMF detector when $P_f = 0.01$ and $J = 4$. (b) "Zoomed-in" version of (a).

So far we have assumed that the model order P of the multichannel AR process is known (cf. Assumption AS4). As mentioned in Remark 1 of Section II, various model selection techniques can be used to estimate P, and it is not unusual for these techniques to underestimate or overestimate the model order by a small number (relative to the true model order P) [21, 22]. Hence, it would be of interest to find out how the parametric Rao/PAMF detector performs when an inaccurate model order estimate is used. This is shown in Fig. 7, where the performance of the Rao/PAMF detector using the true, an underestimated, and an overestimated model order is depicted. As we can see, using an inaccurate model order estimate degrades the detection performance, but the degradation is not significant, especially in the case of model order overestimation. Overestimation is a more robust error since the high-order coefficients can be estimated close to zero (providing that the size of the signals that can be used for estimation is large enough). The above behavior of the parametric Rao/PAMF detector is typical and has been consistently observed in other experiments with a similar setup. Here, we only considered the case where the model order is incorrectly estimated by one unit. A larger performance variation is expected if there is a larger estimation error for P.

Finally, Fig. 8 depicts P_d versus SINR for the parametric Rao/PAMF detector when $J = 4$, $P_f = 0.01$,

and N varies from $N = 4$ to $N = 128$. It is seen that the detection performance increases with N.

VI. CONCLUSIONS

We have developed a parametric Rao test for the multichannel adaptive signal detection problem by exploiting a multichannel AR model. We have derived the ML estimates of the parameters involved in the test. The parametric Rao test is an asymptotic parametric GLRT, and the asymptotic distributions of its test statistic under both hypotheses have been obtained in closed form. We have shown that the PAMF test statistic has a form identical to that of the parametric Rao test statistic; therefore, the PAMF test is also an asymptotic parametric GLRT. Computer simulations show that: 1) our asymptotic analysis provides fairly accurate prediction of the performance of the parametric Rao/PAMF test; 2) even with relatively limited training, the parametric Rao/PAMF detector is quite close to the ideal MF detector; 3) the parametric Rao/PAMF detector outperforms the AMF detector, which does not exploit a parametric model; and finally 4) the performance of the parametric Rao/PAMF detector is affected by inaccurate model order estimation, but the resulting performance degradation is tolerable when the model order estimation error is small.

Our asymptotic analysis of the parametric Rao detector is based on several assumptions stated in Section II, including that the disturbance can be modeled as an AR(P) process with known model order P, and that the training signals are IID When these assumptions are violated, we expect that the analysis will be less accurate, but may still be informative if the assumptions are not significantly violated. For example, we have noticed in simulation that when the disturbance is an MA process, the test threshold obtained by analysis assuming an AR model is still quite accurate. One possible reason is that AR models are fairly general parametric models, and under mild conditions, can be used to model or approximate a large class of stationary random processes (e.g., an MA process can be approximated as an AR process with a high enough model order) [23]. Nevertheless, there is a need to find out how accurate our analysis is in real systems with real data, when the assumptions of Section II may not all be met. This will be an interesting future effort.

APPENDIX A. ML PARAMETER ESTIMATION

In the following, we derive the ML estimates of the nuisance parameters $\mathbf{Q}$ and $\{\mathbf{A}(p)\}_{p=1}^{P}$ or $\mathbf{A}$ defined in (21) under H_0, which is needed in the derivation of the Rao test in Appendix B. The joint probability density function (pdf) or likelihood function $\prod_k f_i(\mathbf{x}_k(0),\mathbf{x}_k(1),\ldots,\mathbf{x}_k(N-1);\alpha,\mathbf{A},\mathbf{Q})$ under H_i, $i = 0$ or 1, can be written as

$$\prod_k f_i(\mathbf{x}_k(P),\mathbf{x}_k(P+1),\ldots,\mathbf{x}_k(N-1)\mid \mathbf{x}_k(0),\mathbf{x}_k(1),\ldots,\mathbf{x}_k(P-1);\mathbf{A},\mathbf{Q}) f(\mathbf{x}_k(0),\mathbf{x}_k(1),\ldots,\mathbf{x}_k(P-1);\alpha,\mathbf{A},\mathbf{Q}). \tag{36}$$

The exact maximization of the pdf with respect to the unknown parameters produces a set of highly nonlinear equations that are difficult to solve. For large data records, the likelihood function can be approximated well by the conditional pdf in the above equation [21] and, therefore, the latter can be used for parameter estimation. After some manipulations using the standard procedure for obtaining the pdf of a set of transformed random variables, we have

$$f_i(\mathbf{x}_k(P),\mathbf{x}_k(P+1),\ldots,\mathbf{x}_k(N-1)\mid \mathbf{x}_k(0),\mathbf{x}_k(1),\ldots,\mathbf{x}_k(P-1);\alpha,\mathbf{A},\mathbf{Q}) = \prod_{n=P}^{N-1}\frac{1}{\pi^J|\mathbf{Q}|}\exp\{-\boldsymbol{\varepsilon}_k^{\mathrm{H}}(n)\mathbf{Q}^{-1}\boldsymbol{\varepsilon}_k(n)\} \tag{37}$$

where for $k \geq 1$, $\boldsymbol{\varepsilon}_k(n)$ is a function of the observed signals given by (7), whereas $\boldsymbol{\varepsilon}_0(n)$ is given by (8) or (11) with $\alpha = 0$ when $i = 0$ and $\alpha \neq 0$ when $i = 1$.

Recall that the training signals $\{\mathbf{x}_k\}_{k=1}^{K}$ and the test signal $\mathbf{x}_0$ are independent. Let $\mathbf{X}(n) = [\mathbf{x}_0^{\mathrm{T}}(n),\mathbf{x}_1^{\mathrm{T}}(n),\mathbf{x}_2^{\mathrm{T}}(n),\ldots,\mathbf{x}_K^{\mathrm{T}}(n)]^{\mathrm{T}}$. The joint conditional pdf is given by

$$\begin{aligned} f_i(\mathbf{X}(P),\mathbf{X}(P+1),\ldots,\mathbf{X}(N-1)\mid \mathbf{X}(0),\mathbf{X}(1),\ldots,\mathbf{X}(P-1);\alpha,\mathbf{A},\mathbf{Q}) &= f_i(\alpha,\mathbf{A},\mathbf{Q}) \\ &= \left[\frac{1}{\pi^J|\mathbf{Q}|}\exp\{-\mathrm{tr}(\mathbf{Q}^{-1}\mathbf{Q}_i(\mathbf{A}))\}\right]^{(K+1)(N-P)} \end{aligned} \tag{38}$$

where in the first equality we dropped the dependence on the observed signals for notational brevity,

$$\mathbf{Q}_i(\alpha,\mathbf{A}) = \frac{1}{(K+1)(N-P)}\sum_{n=P}^{N-1}\sum_{k=0}^{K}\boldsymbol{\varepsilon}_k(n)\boldsymbol{\varepsilon}_k^{\mathrm{H}}(n) \tag{39}$$

and we reiterate that $\alpha = 0$ for $i = 0$, $\alpha \neq 0$ for $i = 1$, and $\boldsymbol{\varepsilon}_0(n)$ depends on α as shown in (8) or (11).

The Rao test requires the ML estimates of the nuisance parameters under H_0. Henceforth, we only consider the case $i = 0$. Taking the derivative of $\ln f_0(\mathbf{A},\mathbf{Q})$ with respect to $\mathbf{Q}$ and equating the result to zero produces the ML estimates of $\mathbf{Q}(\mathbf{A})$ given $\mathbf{A}$:[4]

$$\hat{\mathbf{Q}}_{\mathrm{ML}}(\mathbf{A}) = \mathbf{Q}_0(\mathbf{A}). \tag{40}$$

[4]Since $\alpha = 0$ for $i = 0$, the dependence on α is dropped.

Substituting $\hat{\mathbf{Q}}_{\mathrm{ML}}(\mathbf{A})$ into $f_0(\mathbf{A},\mathbf{Q})$, we have

$$\max_{\mathbf{Q}} f_0(\mathbf{A},\mathbf{Q}) = \left[\frac{1}{(e\pi)^J |\mathbf{Q}_0(\mathbf{A})|}\right]^{(K+1)(N-P)}. \quad (41)$$

Next, we determine the ML estimates of $\mathbf{A}$. Since maximizing $f_0(\mathbf{A})$ is equivalent to minimizing $|\hat{\mathbf{Q}}_{\mathrm{ML}}(\mathbf{A})|$, or $|\mathbf{Q}_0(\mathbf{A})|$, the ML estimate of $\mathbf{A}$ can be obtained by minimizing $|\mathbf{Q}_0(\mathbf{A})|$ with respect to $\mathbf{A}$. We next expand the matrix as follows:

$$\begin{aligned}(K+1)(N-P)&\mathbf{Q}_0(\mathbf{A})\\ &= \hat{\mathbf{R}}_{xx} + \mathbf{A}^{\mathrm{H}}\hat{\mathbf{R}}_{yx} + \hat{\mathbf{R}}_{yx}^{\mathrm{H}}\mathbf{A} + \mathbf{A}^{\mathrm{H}}\hat{\mathbf{R}}_{yy}\mathbf{A}\\ &= (\mathbf{A}^{\mathrm{H}} + \hat{\mathbf{R}}_{yx}^{\mathrm{H}}\hat{\mathbf{R}}_{yy}^{-1})\hat{\mathbf{R}}_{yy}(\mathbf{A}^{\mathrm{H}} + \hat{\mathbf{R}}_{yx}^{\mathrm{H}}\hat{\mathbf{R}}_{yy}^{-1})^{\mathrm{H}}\\ &\quad + \hat{\mathbf{R}}_{xx} - \hat{\mathbf{R}}_{yx}^{\mathrm{H}}\hat{\mathbf{R}}_{yy}^{-1}\hat{\mathbf{R}}_{yx} \end{aligned} \quad (42)$$

where the correlation matrices are defined in (23)–(25). Since $\hat{\mathbf{R}}_{yy}$ is nonnegative definite and the remaining terms in (42) do not depend on $\mathbf{A}$, it follows that[5]

$$\mathbf{Q}_0(\mathbf{A}) \geq \mathbf{Q}_0(\mathbf{A})|_{\mathbf{A}=\hat{\mathbf{A}}} \quad (43)$$

where

$$\hat{\mathbf{A}}^{\mathrm{H}} = -\hat{\mathbf{R}}_{yx}^{\mathrm{H}}\hat{\mathbf{R}}_{yy}^{-1}. \quad (44)$$

When $\mathbf{Q}_0(\mathbf{A})$ is minimized, the estimate $\hat{\mathbf{A}}^{\mathrm{H}}$ of $\mathbf{A}^{\mathrm{H}}$ will minimize any nondecreasing function including the determinant of $\mathbf{Q}_0(\mathbf{A})$ [24]. Hence, the ML estimate $\hat{\mathbf{A}}_{\mathrm{ML}}^{\mathrm{H}}$ of $\mathbf{A}^{\mathrm{H}}$ is given by (44) or (26), and $\hat{\mathbf{Q}}_{\mathrm{ML}}$ is given by (27), which is obtained by replacing $\mathbf{A}^{\mathrm{H}}$ in (42) with $\hat{\mathbf{A}}_{\mathrm{ML}}^{\mathrm{H}}$. The subscript "ML" is dropped in other parts of the paper for notational brevity.

APPENDIX B. DERIVATION OF THE PARAMETRIC RAO TEST

The composite hypothesis testing problem (3) involves a signal parameter vector $\boldsymbol{\theta}_r = [\alpha_R, \alpha_I]^{\mathrm{T}} = [\Re\{\alpha\}, \Im\{\alpha\}]^{\mathrm{T}}$ and a nuisance parameter vector $\boldsymbol{\theta}_s$ that includes all unknown parameters in $\{\mathbf{A}^{\mathrm{H}}(p)\}_{p=1}^{P}$ and $\mathbf{Q}$. The nuisance parameter vector $\boldsymbol{\theta}_s$ may be written as $\boldsymbol{\theta}_s = [\mathbf{q}_R^{\mathrm{T}}, \mathbf{q}_I^{\mathrm{T}}, \mathbf{a}_R^{\mathrm{T}}, \mathbf{a}_I^{\mathrm{T}}]^{\mathrm{T}}$ with $\mathbf{a}_R = \mathrm{vec}(\Re\{\mathbf{A}^{\mathrm{H}}\})$, $\mathbf{a}_I = \mathrm{vec}(\Im\{\mathbf{A}^{\mathrm{H}}\})$, $\mathbf{q}_R$ contains the diagonal elements in $\mathbf{Q}$ and the real part of the elements below the diagonal, while $\mathbf{q}_I$ contains the imaginary part of the elements below the diagonal (note that the spatial covariance matrix $\mathbf{Q}$ is a Hermitian matrix). Let

$$\boldsymbol{\theta} = [\boldsymbol{\theta}_r^{\mathrm{T}}, \boldsymbol{\theta}_s^{\mathrm{T}}]^{\mathrm{T}}. \quad (45)$$

Observing that the nuisance parameters are the same under both hypotheses, we can write the parameter test as follows:

$$\begin{aligned} H_0 &: \quad \boldsymbol{\theta}_r = \boldsymbol{\theta}_{r_0}, \boldsymbol{\theta}_s\\ H_1 &: \quad \boldsymbol{\theta}_r = \boldsymbol{\theta}_{r_1}, \boldsymbol{\theta}_s \end{aligned} \quad (46)$$

[5]For two nonnegative definite matrices $\mathbf{A}$ and $\mathbf{B}$, we have $\mathbf{A} \geq \mathbf{B}$ if $\mathbf{A} - \mathbf{B}$ is nonnegative definite.

where $\boldsymbol{\theta}_{r_0} = [0,0]^{\mathrm{T}}$ and $\boldsymbol{\theta}_{r_1} = \boldsymbol{\theta}_r = [\alpha_R, \alpha_I]^{\mathrm{T}}$. The pdf under H_0 and the pdf under H_1 differ only in the value of $\boldsymbol{\theta}$, and they are given by (see Appendix A):

$$f_i(\boldsymbol{\theta}) = \left[\frac{1}{\pi^J |\mathbf{Q}|}\exp\{-\mathrm{tr}(\mathbf{Q}^{-1}\mathbf{Q}_i(\alpha,\mathbf{A}))\}\right]^{(K+1)(N-P)}$$

where $\mathbf{Q}_i(\alpha,\mathbf{A})$ is defined in (39). The Rao test is given by [7]

$$\left.\frac{\partial \ln f(\boldsymbol{\theta})}{\partial \boldsymbol{\theta}_r}\right|_{\boldsymbol{\theta}=\tilde{\boldsymbol{\theta}}}^{\mathrm{T}} [\mathbf{I}^{-1}(\tilde{\boldsymbol{\theta}})]_{\boldsymbol{\theta}_r,\boldsymbol{\theta}_r} \left.\frac{\partial \ln f(\boldsymbol{\theta})}{\partial \boldsymbol{\theta}_r}\right|_{\boldsymbol{\theta}=\tilde{\boldsymbol{\theta}}} \underset{H_0}{\overset{H_1}{\gtrless}} \gamma_{\mathrm{Rao}} \quad (47)$$

where γ_{Rao} denotes a corresponding threshold,

$$\tilde{\boldsymbol{\theta}} = [\boldsymbol{\theta}_{r_0}^{\mathrm{T}}, \hat{\boldsymbol{\theta}}_{s_0}^{\mathrm{T}}]^{\mathrm{T}} \quad (48)$$

denotes the ML estimate of $\boldsymbol{\theta}$ under H_0, and

$$[\mathbf{I}^{-1}(\boldsymbol{\theta})]_{\boldsymbol{\theta}_r,\boldsymbol{\theta}_r} = [\mathbf{I}_{\boldsymbol{\theta}_r,\boldsymbol{\theta}_r}(\boldsymbol{\theta}) - \mathbf{I}_{\boldsymbol{\theta}_r,\boldsymbol{\theta}_s}(\boldsymbol{\theta})\mathbf{I}_{\boldsymbol{\theta}_s,\boldsymbol{\theta}_s}^{-1}(\boldsymbol{\theta})\mathbf{I}_{\boldsymbol{\theta}_s,\boldsymbol{\theta}_r}(\boldsymbol{\theta})]^{-1} \quad (49)$$

which is related to the Fisher information matrix (FIM), given by [7]

$$\mathbf{I}(\boldsymbol{\theta}) = \begin{bmatrix} \mathbf{I}_{\boldsymbol{\theta}_r,\boldsymbol{\theta}_r}(\boldsymbol{\theta}) & \mathbf{I}_{\boldsymbol{\theta}_r,\boldsymbol{\theta}_s}(\boldsymbol{\theta}) \\ \mathbf{I}_{\boldsymbol{\theta}_s,\boldsymbol{\theta}_r}(\boldsymbol{\theta}) & \mathbf{I}_{\boldsymbol{\theta}_s,\boldsymbol{\theta}_s}(\boldsymbol{\theta}) \end{bmatrix}. \quad (50)$$

Hence, the problem boils down to finding the ML estimates of the nuisance parameters under H_0, which have been obtained in Appendix A, and evaluating the first-order derivatives of the log likelihood and the FIM at the ML estimates of the nuisance parameters. The latter task is worked out next.

The FIM is block diagonal. To see this, let q_{R_i}, q_{I_i}, a_{R_i}, and a_{I_i} denote the ith element of $\mathbf{q}_R$, $\mathbf{q}_I$, $\mathbf{a}_R$ and $\mathbf{a}_I$, respectively. The first partial derivative of the log likelihood $\ln f$ with respect to (w.r.t.) α_R is

$$\frac{\partial \ln f}{\partial \alpha_R} = \sum_{n=P}^{N-1} \tilde{\mathbf{s}}^{\mathrm{H}}(n)\mathbf{Q}^{-1}\varepsilon_0(n) + \sum_{n=P}^{N-1} \varepsilon_0^{\mathrm{H}}(n)\mathbf{Q}^{-1}\tilde{\mathbf{s}}(n). \quad (51)$$

The second partial derivative of $\ln f$ w.r.t. α_R and q_{R_i} becomes

$$\frac{\partial^2 \ln f}{\partial \alpha_R \partial q_{R_i}} = -2\Re\left\{\sum_{n=P}^{N-1} \varepsilon_0^{\mathrm{H}}(n)\mathbf{Q}^{-1}\frac{\partial \mathbf{Q}}{\partial q_{R_i}}\mathbf{Q}^{-1}\tilde{\mathbf{s}}(n)\right\}. \quad (52)$$

Likewise, we have

$$\frac{\partial^2 \ln f}{\partial \alpha_R \partial q_{I_i}} = -2\Im\left\{\sum_{n=P}^{N-1} \tilde{\mathbf{s}}^{\mathrm{H}}(n)\mathbf{Q}^{-1}\frac{\partial \mathbf{Q}}{\partial q_{I_i}}\mathbf{Q}^{-1}\varepsilon_0(n)\right\} \quad (53)$$

and

$$\frac{\partial^2 \ln f}{\partial \alpha_R \partial a_{R_i}} = 2\sum_{n=P}^{N-1}\sum_{p=1}^{P} \Re\left\{ \alpha \varepsilon_0^{\mathrm{H}}(n)\mathbf{Q}^{-1}\frac{\partial \mathbf{A}^{\mathrm{H}}(p)}{\partial a_{R_i}}\mathbf{s}(n-p) + \tilde{\mathbf{s}}^{\mathrm{H}}(n)\mathbf{Q}^{-1}\frac{\partial \mathbf{A}^{\mathrm{H}}(p)}{\partial a_{R_i}} \times [\mathbf{x}_0(n-p) - \alpha \mathbf{s}(n-p)] \right\}. \quad (54)$$

Since $E[\mathbf{x}_0(n) - \alpha\mathbf{s}(n)] = E[\mathbf{x}_0(n-p) - \alpha\mathbf{s}(n-p)] = 0$ and $E[\varepsilon_0(n)] = 0$, taking the expectation in (52)–(54) yields

$$E\left[\frac{\partial^2 \ln f}{\partial \alpha_R \partial q_{R_i}}\right] = E\left[\frac{\partial^2 \ln f}{\partial \alpha_R \partial q_{I_i}}\right] = E\left[\frac{\partial^2 \ln f}{\partial \alpha_R \partial a_{R_i}}\right] = 0. \quad (55)$$

In a similar way, we can show

$$E\left[\frac{\partial^2 \ln f}{\partial \alpha_I \partial q_{R_i}}\right] = E\left[\frac{\partial^2 \ln f}{\partial \alpha_I \partial q_{I_i}}\right] = E\left[\frac{\partial^2 \ln f}{\partial \alpha_R \partial a_{I_i}}\right] = E\left[\frac{\partial^2 \ln f}{\partial \alpha_I \partial a_{R_i}}\right] = E\left[\frac{\partial^2 \ln f}{\partial \alpha_I \partial a_{I_i}}\right] = 0. \quad (56)$$

Summarizing the above calculations, we have

$$\mathbf{I}_{\boldsymbol{\theta}_r,\boldsymbol{\theta}_s}(\boldsymbol{\theta}) = \mathbf{0}, \qquad \mathbf{I}_{\boldsymbol{\theta}_s,\boldsymbol{\theta}_r}(\boldsymbol{\theta}) = \mathbf{0} \quad (57)$$

which implies that the FIM is block diagonal. It follows that

$$[\mathbf{I}^{-1}(\tilde{\boldsymbol{\theta}})]_{\boldsymbol{\theta}_r,\boldsymbol{\theta}_r} = \mathbf{I}^{-1}_{\boldsymbol{\theta}_r,\boldsymbol{\theta}_r}(\tilde{\boldsymbol{\theta}}). \quad (58)$$

Hence, we only need to compute $\mathbf{I}^{-1}_{\boldsymbol{\theta}_r,\boldsymbol{\theta}_r}(\tilde{\boldsymbol{\theta}})$, which is obtained next.

The second partial derivative of $\ln f$ w.r.t. α_R is

$$\frac{\partial^2 \ln f}{\partial \alpha_R^2} = -2\sum_{n=P}^{N-1} \tilde{\mathbf{s}}^{\mathrm{H}}(n)\mathbf{Q}^{-1}\tilde{\mathbf{s}}(n). \quad (59)$$

Likewise, we have

$$\frac{\partial^2 \ln f}{\partial \alpha_I^2} = -2\sum_{n=P}^{N-1} \tilde{\mathbf{s}}^{\mathrm{H}}(n)\mathbf{Q}^{-1}\tilde{\mathbf{s}}(n) \quad (60)$$

and

$$\frac{\partial^2 \ln f}{\partial \alpha_R \partial \alpha_I} = \frac{\partial^2 \ln f}{\partial \alpha_I \partial \alpha_R} = 0. \quad (61)$$

As a result, we have the FIM associated with the signal parameter vector:

$$\mathbf{I}_{\boldsymbol{\theta}_r,\boldsymbol{\theta}_r}(\boldsymbol{\theta}) = 2\sum_{n=P}^{N-1} \tilde{\mathbf{s}}^{\mathrm{H}}(n)\mathbf{Q}^{-1}\tilde{\mathbf{s}}(n)\begin{bmatrix}1 & 0\\ 0 & 1\end{bmatrix}. \quad (62)$$

Finally, by inverting the matrix (62) and replacing $\boldsymbol{\theta}$ with $\tilde{\boldsymbol{\theta}}$ which is the ML estimate of $\boldsymbol{\theta}$ under H_0, we have

$$\mathbf{I}^{-1}_{\boldsymbol{\theta}_r,\boldsymbol{\theta}_r}(\tilde{\boldsymbol{\theta}}) = \frac{1}{2\sum_{n=P}^{N-1} \hat{\tilde{\mathbf{s}}}^{\mathrm{H}}(n)\hat{\mathbf{Q}}^{-1}\hat{\tilde{\mathbf{s}}}(n)}\begin{bmatrix}1 & 0\\ 0 & 1\end{bmatrix} \quad (63)$$

where $\hat{\mathbf{Q}}$ is the ML estimate of the spatial covariance matrix in (27), and $\hat{\tilde{\mathbf{s}}}(n)$ is the temporally whitened steering vector in (19). Moreover, since $\varepsilon_0(n)|_{\boldsymbol{\theta}=\tilde{\boldsymbol{\theta}}} = \hat{\tilde{\mathbf{x}}}_0(n)$, we have

$$\left.\frac{\partial \ln f}{\partial \alpha_R}\right|_{\boldsymbol{\theta}=\tilde{\boldsymbol{\theta}}} = \sum_{n=P}^{N-1}\{\hat{\tilde{\mathbf{x}}}_0^{\mathrm{H}}(n)\hat{\mathbf{Q}}^{-1}\hat{\tilde{\mathbf{s}}}(n) + \hat{\tilde{\mathbf{s}}}^{\mathrm{H}}(n)\hat{\mathbf{Q}}^{-1}\hat{\tilde{\mathbf{x}}}_0(n)\} \quad (64)$$

$$\left.\frac{\partial \ln f}{\partial \alpha_I}\right|_{\boldsymbol{\theta}=\tilde{\boldsymbol{\theta}}} = j\sum_{n=P}^{N-1}\{\hat{\tilde{\mathbf{x}}}_0^{\mathrm{H}}(n)\hat{\mathbf{Q}}^{-1}\hat{\tilde{\mathbf{s}}}(n) + \hat{\tilde{\mathbf{s}}}^{\mathrm{H}}(n)\hat{\mathbf{Q}}^{-1}\hat{\tilde{\mathbf{x}}}_0(n)\}. \quad (65)$$

Using (63)–(65) in (47) yields the parametric Rao test, which is shown in (18).

APPENDIX C. ASYMPTOTIC DISTRIBUTION OF THE PARAMETRIC RAO TEST STATISTIC

The Rao test is known to have the same asymptotic performance as the GLRT. Using the asymptotic results for the GLRT [7], the asymptotic distribution of our parametric Rao test statistic is given by

$$T_{\mathrm{Rao}} \overset{a}{\sim} \begin{cases} \chi_2^2, & \text{under } H_0 \\ \chi_2'^2(\lambda), & \text{under } H_1 \end{cases} \quad (66)$$

where χ_2^2 denotes the central Chi-squared distribution with 2 degrees of freedom and $\chi_2'^2(\lambda)$ the noncentral Chi-squared distribution with 2 degrees of freedom and noncentrality parameter λ:

$$\lambda = (\boldsymbol{\theta}_{r_1} - \boldsymbol{\theta}_{r_0})^{\mathrm{T}}([\mathbf{I}^{-1}([\boldsymbol{\theta}_{r_0}, \boldsymbol{\theta}_s])]_{\boldsymbol{\theta}_r,\boldsymbol{\theta}_r})^{-1}(\boldsymbol{\theta}_{r_1} - \boldsymbol{\theta}_{r_0}). \quad (67)$$

Using the observations $\boldsymbol{\theta}_{r_1} - \boldsymbol{\theta}_{r_0} = [\alpha_R, \alpha_I]$ and (cf. (62))

$$[\mathbf{I}^{-1}([\boldsymbol{\theta}_{r_0}, \boldsymbol{\theta}_s])]_{\boldsymbol{\theta}_r,\boldsymbol{\theta}_r} = \frac{1}{2\sum_{n=P}^{N-1} \tilde{\mathbf{s}}^{\mathrm{H}}(n)\mathbf{Q}^{-1}\tilde{\mathbf{s}}(n)}\begin{bmatrix}1 & 0\\ 0 & 1\end{bmatrix} \quad (68)$$

we have the asymptotic distribution of the parametric Rao test statistic as shown in (28).

APPENDIX D. PERFORMANCE OF THE MF AND AMF DETECTORS

The performance of the MF and AMF detectors can be computed analytically. In this appendix, we include a brief summary of their performance for easy reference.

Consider the MF detector (12) first. Let $\mathbf{R}^{-1/2}$ be the square root of the space-time covariance matrix $\mathbf{R}$. Define $\tilde{\mathbf{s}} = \mathbf{R}^{-1/2}\mathbf{s}$ and $\tilde{\mathbf{x}}_0 = \mathbf{R}^{-1/2}\mathbf{x}_0$, which are the spatially and temporally whitened steering vector and

test signal, respectively. Since the rank of $\tilde{\mathbf{s}}\tilde{\mathbf{s}}^{\mathrm{H}}$ is one, we have the following eigen decomposition:

$$\tilde{\mathbf{s}}\tilde{\mathbf{s}}^{\mathrm{H}} = \mathbf{U}\boldsymbol{\Lambda}\mathbf{U}^{\mathrm{H}} \tag{69}$$

where $\boldsymbol{\Lambda} = \mathrm{diag}(\tilde{\mathbf{s}}^{\mathrm{H}}\tilde{\mathbf{s}}, 0, \ldots, 0)$ and $\mathbf{U}^{\mathrm{H}}\mathbf{U} = \mathbf{I}$. Let $\bar{\mathbf{x}}_0 = \mathbf{U}^{\mathrm{H}}\tilde{\mathbf{x}}_0$ and $\bar{\mathbf{s}} = \mathbf{U}^{\mathrm{H}}\tilde{\mathbf{s}}$, which are rotated versions of $\tilde{\mathbf{x}}_0$ and $\tilde{\mathbf{s}}$, respectively. Then, the test statistic can be written as

$$T_{\mathrm{MF}} = \frac{|\tilde{\mathbf{s}}^{\mathrm{H}}\tilde{\mathbf{x}}_0|^2}{\tilde{\mathbf{s}}^{\mathrm{H}}\tilde{\mathbf{s}}} = \frac{\tilde{\mathbf{x}}_0^{\mathrm{H}}\mathbf{U}\boldsymbol{\Lambda}\mathbf{U}^{\mathrm{H}}\tilde{\mathbf{x}}_0}{\tilde{\mathbf{s}}^{\mathrm{H}}\tilde{\mathbf{s}}} = \bar{x}_{0,1}^{*}\bar{x}_{0,1} = |\bar{x}_{0,1}|^2 \tag{70}$$

where $\bar{x}_{0,1}$ and $\bar{s}_1$ denote the first element of $\bar{\mathbf{x}}_0$ and $\bar{\mathbf{s}}$, respectively. It is clear from Assumptions AS1–AS3 in Section II that $\bar{x}_{0,1}$ is a complex Gaussian variable: $\bar{x}_{0,1} \sim \mathcal{CN}(\alpha\bar{s}_1, 1)$ with $\alpha = 0$ under H_0 and $\alpha \neq 0$ under H_1. Hence, $2T_{\mathrm{MF}} = 2|\bar{x}_{0,1}|^2$ has a central Chi-squared distribution with 2 degrees of freedom under H_0 and, respectively, a noncentral Chi-squared distribution with 2 degrees of freedom and a noncentrality parameter $\lambda_{\mathrm{MF}} = 2|\alpha\bar{s}_1|^2$ under H_1. It is noted that the distribution of the MF test statistic is similar to that of the parametric Rao test statistic with the only difference of the noncentrality parameter under H_1. Hence, the false alarm and detection probabilities can be similarly computed as in (33) and (34).

The performance of the AMF detector (14) was analyzed in [12], which is summarized below. The density of a loss factor ρ, which was defined in [12, eq. (25)], is given by

$$f(\rho) = f_\beta(\rho; L-1, JN-1) \tag{71}$$

where $L = K - JN + 1$ and the central Beta density function is

$$f_\beta(x; n, m) = \frac{(n+m-1)!}{(n-1)!(m-1)!}x^{n-1}(1-x)^{m-1}. \tag{72}$$

The probability of false alarm is given by

$$P_{\mathrm{f,AMF}} = \int_0^1 \frac{f_\beta(\rho; L-1, JN-1)}{(1+\eta\rho)^L}d\rho \tag{73}$$

where $\eta = \gamma_{\mathrm{Kelly}}/(1-\gamma_{\mathrm{Kelly}})$ and γ_{Kelly} is the test threshold of Kelly's GLRT (15). Meanwhile, the probability of detection is given by

$$P_{\mathrm{d,AMF}} = 1 - \int_0^1 \frac{1}{(1+\eta\rho)^L}\sum_{m=1}^{L}\binom{L}{m} \times (\eta\rho)^m G_m\left(\frac{\xi\rho}{1+\eta\rho}\right)f(\rho)d\rho \tag{74}$$

where $\xi = \mathbf{s}^{\mathrm{H}}\mathbf{R}^{-1}\mathbf{s}$ and $G_m(\cdot)$ is the incomplete Gamma function given by

$$G_m(y) = e^{-y}\sum_{k=0}^{m-1}\frac{y^k}{k!}. \tag{75}$$

The integrals can be computed by numerical integration.

REFERENCES

[1] Ward, J.
Space-time adaptive processing for airborne radar.
Lincoln Laboratory, MIT, Technical Report 1015, Dec. 1994.

[2] Klemm, R.
Principles of Space-Time Adaptive Processing.
London: The Institute of Electrical Engineers, 2002.

[3] Shaw, G., and Manolakis, D.
Signal processing for hyperspectral image exploitation.
IEEE Signal Processing Magazine, **19**, 1 (Jan. 2002), 12–16.

[4] Manolakis, D., and Shaw, G.
Detection algorithms for hyperspectral imaging applications.
IEEE Signal Processing Magazine, **19**, 1 (Jan. 2002), 29–43.

[5] Paulraj, A., and Papadias, C. B.
Space-time processing for wireless communications.
IEEE Signal Processing Magazine, **14** (Nov. 1997), 49–83.

[6] Justice, J. H.
Array processing in exploration seismology.
In S. Haykin (Ed.), *Array Signal Processing*, Englewood Cliffs, NJ: Prentice-Hall, 1985.

[7] Kay, S. M.
Fundamentals of Statistical Signal Processing: Detection Theory.
Englewood Cliffs, NJ: Prentice-Hall, 1998.

[8] Reed, I. S., Mallett, J. D., and Brennan, L. E.
Rapid convergence rate in adaptive arrays.
IEEE Transactions on Aerospace and Electronic Systems, **10**, 6 (1974), 853–863.

[9] Kelly, E. J.
An adaptive detection algorithm.
IEEE Transactions on Aerospace and Electronic Systems, **22** (Mar. 1986), 115–127.

[10] Cai, L., and Wang, H.
On adaptive filtering with the CFAR feature and its performance sensitivity to non-Gaussian interference.
In *Proceedings of the 24th Annul Conference on Information Sciences and Systems*, Princeton, NJ, Mar. 1990, 558–563.

[11] Chen, W., and Reed, I. S.
A new CFAR detection test for radar.
Digital Signal Processing, **1**, 4 (1991), 198–214.

[12] Robey, F. C., Fuhrmann, D. R., Kelly, E. J., and Nitzberg, R.
A CFAR adaptive matched filter detector.
IEEE Transactions on Aerospace and Electronic Systems, **28**, 1 (Jan. 1992), 208–216.

[13] Kraut, S., and Scharf, L. L.
The CFAR adaptive subspace detector is a scale-invariant GLRT.
IEEE Transactions on Signal Processing, **47**, 9 (Sept. 1999), 2538–2541.

[14] Kraut, S., Scharf, L. L., and McWhorter, L. T.
Adaptive subspace detectors.
IEEE Transactions on Signal Processing, **49**, 1 (Jan. 2001), 1–16.

[15] Rangaswamy, M., and Michels, J. H.
A parametric multichannel detection algorithm for correlated non-Gaussian random processes.
In *Proceedings of the 1997 IEEE National Radar Conference*, Syracuse, NY, May 1997, 349–354.

[16] Román, J. R., Rangaswamy, M., Davis, D. W., Zhang, Q., Himed, B., and Michels, J. H.
Parametric adaptive matched filter for airborne radar applications.
IEEE Transactions on Aerospace and Electronic Systems, **36**, 2 (Apr. 2000), 677–692.

[17] Swindlehurst, A. L., and Stoica, P.
Maximum likelihood methods in radar array signal processing.
Proceedings of the IEEE, **86** (Feb. 1998), 421–441.

[18] Li, J., Liu, G., Jiang, N., and Stoica, P.
Moving target feature extraction for airborne high-range resolution phased-array radar.
IEEE Transactions on Signal Processing, **49**, 2 (Feb. 2001), 277–289.

[19] Conte, E., and De Maio, A.
Distributed target detection in compound-Gaussian noise with Rao and Wald tests.
IEEE Transactions on Aerospace and Electronic Systems, **39**, 2 (Apr. 2003), 568–582.

[20] De Maio, A., Alfano, G., and Conte, E.
Polarization diversity detection in compound-Gaussian clutter.
IEEE Transactions on Aerospace and Electronic Systems, **40**, 1 (Jan. 2004), 114–131.

[21] Stoica, P., and Moses, R. L.
Spectral Analysis of Signals.
Englewood Cliffs, NJ: Prentice-Hall, 2005.

[22] Tsao, T., Himed, B., and Michels, J. H.
Effects of interference rank estimation on the detection performance of rank reduced STAP algorithms.
In *Proceedings of the 1998 IEEE Radar Conference*, May 1998, 147–152.

[23] Kay, S. M.
Modern Spectral Estimation: Theory and Application.
Englewood Cliffs, NJ: Prentice-Hall, 1988.

[24] Li, J., Halder, B., Stoica, P., and Viberg, M.
Computationally efficient angle estimation for signals with known waveforms.
IEEE Transactions on Signal Processing, **43**, 9 (Sept. 1995), 2154–2163.

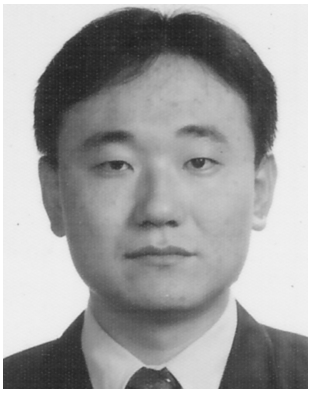

Kwang June Sohn received the B.E. degree in electronics engineering from Kyungpook National University, Daegu, Korea, in 1995, and the M.E. and Ph.D. degrees in electrical engineering from Stevens Institute of Technology, Hoboken, NJ, in 2005 and 2007, respectively.

From 1995 to 1997 he was a research assistant with the Department of Electrical Engineering at Korea Advanced Institute of Science and Technology (KAIST), Daejon, Korea, where he worked for the M.S. degree. In 1997 he joined the Digital Media Laboratory, LG Electronics, Seoul, Korea, where he was involved in the development of DVD player and recorder. From 1999 to 2001 he was a senior software engineer with Korea Telecom Freetel (KTF), Seoul, Korea, where he was involved in the development of the CDMA handset. From 2001 to 2003 he was a senior member of technical staff with KTF where he was responsible for the development and assessment of W-CDMA radio access network and handset. His current research interests lie in the area of statistical signal processing with the applications to radars and wireless communications including detection, estimation, multichannel adaptive signal processing, and space-time adaptive processing.

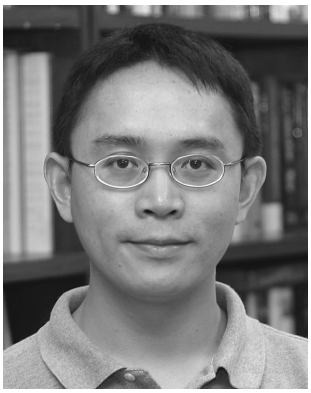

Hongbin Li (M'99) received the B.S. and M.S. degrees from the University of Electronic Science and Technology of China, Chengdu, in 1991 and 1994, respectively, and the Ph.D. degree from the University of Florida, Gainesville, FL, in 1999, all in electrical engineering.

From July 1996 to May 1999, he was a research assistant in the Department of Electrical and Computer Engineering at the University of Florida. He was a summer visiting faculty member at the Air Force Research Laboratory, Rome, NY, in the summers of 2003 and 2004. Since July 1999, he has been with the Department of Electrical and Computer Engineering, Stevens Institute of Technology, Hoboken, NJ, where he is an associate professor. His current research interests include wireless communications and networking, statistical signal processing, and radars.

Dr. Li is a member of Tau Beta Pi and Phi Kappa Phi. He received the Harvey N. Davis Teaching Award in 2003 and the Jess H. Davis Memorial Award for excellence in research in 2001 from Stevens Institute of Technology, and the Sigma Xi Graduate Research Award from the University of Florida in 1999. He is an editor for the *IEEE Transactions on Wireless Communications* and an associate editor for the *IEEE Signal Processing Letters*.

Braham Himed (M'90—SM'01—F'07) received his B.S. degree in electrical engineering from Ecole Nationale Polytechnique of Algiers, Algeria in 1984, and his M.S. and Ph.D. degrees both in electrical engineering, from Syracuse University, Syracuse, NY, in 1987 and 1990, respectively.

From 1990 to 1991 he was an assistant professor in the Electrical Engineering Department at Syracuse University. In 1991 he joined Adaptive Technology, Inc., Syracuse, NY, where he was responsible for radar systems analyses and the analysis and design of antenna measurement systems. In 1994 he joined Research Associates for Defense Conversion, Marcy, NY, where he was responsible for radar systems design and analysis and radar signal processing. From March 1999 to August 2006, he was with the U.S. Air Force Research Laboratory, Sensors Directorate, Radar Signal Processing Branch, Rome, NY, where he was involved with several aspects of airborne and spaceborne phased array radar systems. Since August 2006, he is with Signal Labs, Inc., Reston, VA, where he serves as Chief Research Officer. His research interests include detection, estimation, multichannel adaptive signal processing, time series analyses, array processing, space-time adaptive processing, hot clutter mitigation, and ground penetrating radar technology. Since 1993, he has also been an adjunct professor at Syracuse University.

Dr. Himed is the recipient of the 2001 IEEE region I award for his work on bistatic radar systems, algorithm development and phenomenology. Dr. is a member of the AES Radar Systems Panel.